The Astronomical Journal, 159:208 (11pp), 2020 May https://doi.org/10.3847/1538-3881/ab8004

Intrinsic Color Indices of Early-type Dwarf Stars

Dingshan Deng[1], Yang Sun[1], Mingjie Jian[2], Biwei Jiang[1], and Haibo Yuan[1]
[1] Department of Astronomy, Beijing Normal University, Beijing 100875, People's Republic of China
[2] Department of Astronomy, School of Science, The University of Tokyo, 7-3-1 Hongo, Bunkyo-ku, Tokyo 113-0033, Japan; mingjie@astron.s.u-tokyo.ac.jp
Received 2019 December 7; revised 2020 March 12; accepted 2020 March 13; published 2020 April 14

Abstract

Early-type stars are short lived and scarce in comparison with other types. Based on the recently released catalogs of early-type stars from the largest Large Sky Area Multi-Object Fiber Spectroscopic Telescope spectroscopic survey, the intrinsic colors of the stars with effective temperature up to 32,000 K are determined for the bands from ultraviolet to infrared using the blue-edge method. Analytic relations are derived for the intrinsic color index with the effective temperature for the Wide-field Infrared Survey Explorer, Two Micron All Sky Survey, Gaia, AAVSO Photometric All-Sky Survey, Sloan Digital Sky Survey, the Panoramic Survey Telescope and Rapid Response System 1, and Galaxy Evolution Explorer bands. The results are generally consistent with previous works. In addition, the intrinsic colors of O-type dwarfs and OB supergiants are roughly estimated.

Unified Astronomy Thesaurus concepts: Fundamental parameters of stars (555); Stellar colors (1590); Early-type stars (430)

1. Introduction

Intrinsic color index, or simply called intrinsic color, is a basic stellar parameter related to stellar properties such as atmospheric temperature, metallicity, etc. It can be adopted as a reference in astronomical studies such as in Hertzsprung–Russell diagrams and used to analyze spectral energy distributions (SEDs; Lee 1970; The et al. 1986). Meanwhile, the intrinsic colors are the key to estimate interstellar reddening and extinction, which are important probes of interstellar dust.

Early-type stars, referring to O-, B-, and A-type stars in this work, are very hot and massive stars so that they are short lived. Mostly located in the spiral arms, or other dusty regions from birth, they are usually immersed in dense interstellar clouds. Thus, the number of observable early-type stars are highly limited compared with that of later types. Besides, early-type stars are famous for their strong stellar wind to produce considerable circumstellar material (Garcia-Segura et al. 1996), which brings about uncertainty in determining their stellar properties. Consequently, their intrinsic colors are not well determined.

The intrinsic colors of early-type stars were studied previously by many works in an empirical approach, for example, Johnson (1966), Fitzgerald (1970), Kuriliene & Straizys (1977), Whittet & van Breda (1980), Straizys (1987), and Wegner (1993, 1994, 2014). Although different in details, the principle method adopts two-color diagrams and specific dereddening laws. They used the experimental formula $V-\lambda = a(B-V)+b$, which depends on the assumption that two colors show a linear relationship in some particular range of stellar parameters. Once an intrinsic color index (e.g., $(B-V)_0$) is determined, the other intrinsic colors can be calculated by substituting it into the formula as $(V-\lambda)_0 = a(B-V)_0+b$, where the constants a and b are derived from fitting the observed colors. There are a few problems with this method. First, the linear relation only appears in very limited ranges of stellar parameters and some colors. Figure 2 of Chen et al. (2014) displayed the relation of various intrinsic color indexes with $(g-i)_0$, which clearly showed the variety of the relations even including inverse correlation in some cases, and almost in no case where all the color indexes are linearly related. Second, they need to make their own assumptions or adopt an established dereddening law to determine the first intrinsic color $(B-V)_0$, which would reduce the accuracy. Johnson (1966) assumed that the nearest stars within 100 pc from the Sun were not affected by interstellar extinction and they took the mean value of the observed colors of these stars as intrinsic. In the work of Wegner (1993, 1994, 2014), he adopted the PWK dereddening law from Papaj et al. (1990) while Papaj et al. (1993) found that adopting their dereddening laws brought about some degree of uncertainty. Third, this procedure requires the extinction law to be the same for all the stars in different sightlines or interstellar environments, which may only be valid in some particular regions such as in the OB associations (Krelowski & Strobel 1987). Additionally, the accuracy of intrinsic color is severely affected by the reference color index ($(B-V)_0$ here), i.e., the intrinsic colors are not derived independently.

Meanwhile, synthetic photometry of stellar atmosphere models were utilized to determine the intrinsic colors for early-type stars by other works. In such approach, the effective temperatures ($T_{\rm eff}$) are determined from modeling the spectral features, and the SED of these models can then be convolved with the appropriate sensitivity functions to calculate the intrinsic colors. As an early example, Flower (1975) determined the relationship between $T_{\rm eff}$ and $(B-V)$o for the late-type (M-type) giants and supergiants. Combining with other results (such as Code et al. 1976 for stars with $T_{\rm eff} > 11{,}000$ K), intrinsic colors for supergiants, giants, and dwarfs were presented in Flower (1977). Then, by the aid of the stellar atmosphere models called ATLAS from Kurucz (1979) model, Bessell et al. (1998) determined the intrinsic colors for early-type stars ($T_{\rm eff} > 9000$ K) within the Johnson-Cousins-Glass *UBVJHK* system, and Martins & Plez (2006) performed a similar calculation for O-type stars. In recent years, the stellar atmosphere model generated from PAdova and TRieste Stellar Evolution Code model (PARSEC; Bressan et al. 2012) is popularly used to calculate stellar intrinsic colors for its updated parameters, flexibility, as well as convenient availability online, which is taken into comparison with the present work.

Recently, the so-called blue-edge method is developed to determine stellar intrinsic colors and is applied to all of the stars

except for early spectral types. The idea originated from Ducati et al. (2001), which assumed that the bluest ones in a sample of stars at a given spectral type (and luminosity class) suffer no interstellar extinction and their observed colors are the same as the intrinsic color of this spectral type. This assumption is very reasonable as long as the sample is large enough and includes the zero-reddening stars. This method avoids the shortcomings aforementioned with no assumption on interstellar extinction law or the linear relationship between intrinsic colors. Originally, Ducati et al. (2001) used a catalog of 3946 sources for dwarfs, giants, and subgiants due to the limit of observational data and could only obtain a very rough estimation of stellar intrinsic colors according to their spectral types. With the development of both spectroscopic and photometric observation, significantly larger data sets are collected and this method is developed. With the stellar parameters from the Large Sky Area Multi-Object Fiber Spectroscopic Telescope (LAMOST) and Apache Point Observatory Galactic Evolution Experiment (APOGEE) spectroscopic surveys, Wang & Jiang (2014), Xue et al. (2016), Jian et al. (2017), and Sun et al. (2018) derived the analytic relations of stellar intrinsic colors with $T_{\rm eff}$ in the infrared and ultraviolet bands from the blue edge in the observed color versus $T_{\rm eff}$ diagram, which were used to determine the interstellar extinction law. The accuracy of the blue-edge method depends mainly on the photometric uncertainty (which is unavoidable in any method) and the uncertainty of stellar parameters. The accuracy is generally very high since those two uncertainties are usually small.

However, the early-type stars are not included in these studies of stellar intrinsic colors by the blue-edge method. The key reason lies on the lack of an appropriate sample of early-type stars. Several works have been done to identify OB stars. The Catalog of Galactic OB stars (Reed 2003) collects nearly 16,200 OB stars, including 10,669 OB stars from 12,235 Case-Hamburg Galactic plane luminous-stars and 5500 additional stars from other literature. However, over 8000 of them have no information of spectral classification. Besides, the spectral classification is not based on homogeneous criteria since this is an assembly of various catalogs. The catalog by Gontcharov (2008, 2012) contains 20,514 OV-A0V stars from the Tycho-2 catalog. Because they selected early-type stars from color–color diagrams, no further spectral classification is provided. There must be some contamination of other types of stars as photometry cannot determine the spectral type as convincingly as spectroscopy. According to the tests with Hipparcos Input Catalogue (HIC; Turon et al. 1993) and Tycho-2 Spectral Types (TST) catalog (Wright et al. 2003), 14,732 (94%) of them are of O- to A0-type (Gontcharov 2012). Mohr-Smith et al. (2017) selected 14,900 early-type stars with 5915 high-confidence O-B2 stars with $T_{\rm eff}$ from SED fitting, but these stars are limited in 42 deg^2 in the Carina Arm region with high interstellar extinction. The Galactic O-Star Spectroscopic Survey (GOSSS; Maíz Apellániz et al. 2011; Sota et al. 2014; Maíz Apellániz et al. 2016) is a project dedicated to O-type stars. With a high signal-to-noise ratio (S/N) and the resolution of ∼2500, this survey yields more than 1000 Galactic O stars, which should be the biggest catalog for O stars with spectral classification, though the number of O stars is still limited.

With specific design, the LAMOST has obtained over 10 million stellar spectra. This huge database provides a possibility to expand the catalog of early-type stars, in particular OB stars. Although identifying OB stars is not very difficult, deriving the stellar parameters is hard due to the scarcity of spectral lines and the fact that the LAMOST survey makes no absolute flux calibration. Liu et al. (2019) identified about 16,000 OB stars from the data release 5 (DR5) of the LAMOST survey,[3] the largest ever reliable catalog of the OB stars. Furthermore, C. Liu et al. (2020, in preparation) determined the basic stellar parameters, i.e., $T_{\rm eff}$ and $\log g$, for about 9000 stars in this LAMOST OB star catalog. This newly updated OB star catalog allows us to analyze their intrinsic colors with a much larger sample by the blue-edge method. For the A-type stars with $T_{\rm eff} < 8000$ K whose stellar parameters were derived by the LAMOST pipeline, Jian et al. (2017) already determined their intrinsic colors by the blue-edge method. In order to expand the spectral range coverage, the A-type stars with $T_{\rm eff} > 8000$ K from the LAMOST DR5 value-added catalog (Xiang et al. 2017) are included in this study.

Besides the development of spectroscopic surveys, a number of new photometric surveys are conducted. The most widely used includes the Wide-field Infrared Survey Explorer (WISE), Two Micron All Sky Survey (2MASS), Gaia, AAVSO Photometric All-Sky Survey (APASS), Sloan Digital Sky Survey (SDSS), the Panoramic Survey Telescope (Pan-STARRS1), and Galaxy Evolution Explorer (GALEX) surveys. These surveys use the filters previously undefined, correspondingly the related intrinsic color indexes need to be determined for the early-type stars.

In this work, we determine the intrinsic colors of early-type stars with recently released large catalogs from the LAMOST spectroscopy survey using the blue-edge method for some traditional and innovatory filters. We describe the data in Section 2 and the details of the blue-edge method in Section 3. The result and discussion will be presented in Section 4, and summary in Section 5.

2. Data

Photometric and spectroscopic data are from several large-scale surveys, which gives us the opportunity to collect sufficient data of early-type stars needed for more precise determination of their intrinsic colors.

2.1. Spectroscopic Data

LAMOST (Cui et al. 2012) is a reflective Schmidt telescope at the Xinglong Station of the National Astronomical Observatory of China. We used two catalogs from the LAMOST survey, one of the A-type stars from Xiang et al. (2017) and the other of the OB stars from Liu et al. (2019). They both contain the basic stellar parameters: effective temperature, $T_{\rm eff}$, and surface gravity, $\log g$. The A-type catalog is selected from the LAMOST DR5 value-added catalog (Xiang et al. 2017) with $T_{\rm eff}$ from 8000 to 10,000 K including 205,068 high-temperature A-type stars. We checked the identification of A-type stars of this catalog. First, the catalog is cross-identified with the LAMOST DR5 database which classifies the stars by template match. It is found that 1617 stars are classified as white dwarfs, 98 as quasars, and 995 as galaxies in the LAMOST DR5 database. Moreover, some objects are labeled as "unknown" due to the low S/N spectrum, and some objects are not included in the DR5 database. An additional 188 white dwarfs are recognized by their faintness in Gaia/G ($G > 15$) and close distance with Gaia distance <400 pc, which brings them together in an isolated area in the Gaia/distance–Gaia/G diagram. Altogether, 2898 objects are removed from the A-type catalog of Xiang et al. (2017) for misclassification. The

[3] http://dr5.lamost.org/

OB star catalog is also based on the DR5 but resulted from a dedicated study of the spectral line indices, containing 8582 OB stars (Liu et al. 2019), with $T_{\rm eff}$ ranging within 10,000–32,000 K (C. Liu et al. 2020, in preparation). In addition to $T_{\rm eff}$ and $\log g$, the stellar metallicity [Fe/H] and its error are available as well for the A-type stars, while not for the OB stars.

2.2. Photometric Data

In the optical, we use the data from the Gaia, Pan-STARRS1, APASS, and SDSS surveys. Gaia (Gaia Collaboration et al. 2016) performed all-sky photometric observations in three passbands, G ($\lambda_{\rm eff} = 6730$ Å), $G_{\rm BP}$ (5320 Å), and $G_{\rm RP}$ (7970 Å), with very high accuracy through a wide dynamical range benefited from the space observation. In Gaia DR2 (Gaia Collaboration et al. 2018), its precision in G is about 1 mmag at the bright ($G < 13$) end to around 20 mmag at the faint end ($G = 20$); the precisions in other two bands are a few millimagnitudes at the bright end to around 200 mmag at the faint end. We make no use of the G-band data because the bandwidth is so large that the effective wavelength would be very sensitive to the SED. Pan-STARRS (Chambers et al. 2016) conducted by a 1.8 m telescope in Hawaii surveys in five passbands, g ($\lambda_{\rm eff} = 4866$ Å), r (6215 Å), i (7545 Å), z (8679 Å), and y (9633 Å), which extend the wavelength to infrared adjacent to the common *JHK* bands. The newly released DR2 is used with saturation magnitudes at about 12–14 mag. Since the Johnson system is classical in photometry, it would be convenient to compare with previous works by adding the *UBV* photometric results. For the B and V bands, the APASS DR9 data (Henden & Munari 2014; Henden et al. 2016) is supplemented, which is reliable from about 10.0 mag to 17.0 mag in the V band. Similar to $B - V$, $U - B$ is a widely analyzed color, and more sensitive to $T_{\rm eff}$ for early-type stars. However, the U band is not included in recent photometric surveys so that the data is not sufficient. As a substitution, $(u' - g')_0$ from SDSS DR12 (York et al. 2000; Alam et al. 2015) is analyzed since the SDSS/u' ($\lambda_{\rm eff} = 3596$ Å) and g' (4639 Å) filters are similar to the U (3663 Å) and B (4361 Å) (Bessell 2005), though $(u' - g')_0$ may be bigger than $U - B$ due to a slightly wider wavelength difference between the two filters.

In the infrared, we use the data from the 2MASS and WISE surveys. 2MASS (Skrutskie et al. 2006) is a near-infrared all-sky survey that finished in 2001. The photometric limits in the observed J ($\lambda_{\rm eff} = 1.25$ μm), H (1.65 μm), and K_S (2.17 μm) bands are 15.8, 15.1, and 14.3 mag at an S/N of 5, respectively. WISE is an infrared space telescope launched by NASA in 2009 December (Wright et al. 2010). It surveyed in four bands, W1 ($\lambda_{\rm eff} = 3.35$ μm), W2 (4.60 μm), W3 (11.56 μm), and W4 (22.08 μm) with a bandwidth of 0.66, 1.04, 5.51, and 4.10 μm, respectively. After the WISE all-sky (Cutri & Al 2013) survey, the NEOWISE (an enhanced project of WISE, which aims on near-earth objects (NEOs)) warm mission (Mainzer et al. 2011) only observed in W1 and W2. Consequently, the data in the W3 and W4 bands are fewer than other bands, namely 7628 stars for W3 and 1151 stars for W4 in our sample. Moreover, the photometric quality in W4 is relatively poor, which is not used in further analysis. Fortunately, the SED at wavelengths as long as W4 should be well approximated by the Rayleigh–Jeans law for hot stars, which implies a rather constant color index in the mid- and far-infrared.

For the ultraviolet bands in which the early-type stars are bright, we use the data from GALEX DR6/7 (Martin et al. 2005), which is presently the largest ultraviolet survey. The photometry of GALEX includes two bands, NUV (1750–2800 Å) and FUV (1350–1740 Å), with a limiting magnitude of 21 mag and 20 mag respectively.

The cross-identification between catalogs are performed within a radius of 3″, which is about three times that of the positional uncertainties, although some catalogs like Gaia have higher positional accuracy. The identification should be right when no blending occurs. In cases there are more than one object within this 3″ region centered at the spectroscopic star, the closest one in the photometric data is chosen.

2.3. Data Quality Control

We control the data quality for a precise determination of the intrinsic colors by a compromise between the size and the precision of the sample. Since every catalog has its own claimed errors, our criteria to filter the data coincide with these errors. For the photometric catalogs, the data are cut within the error of 0.01 mag, 0.05 mag, 0.02 mag, 0.03 mag, 0.03 mag, 0.05 mag, 0.1 mag, and 0.05 mag respectively for Gaia, SDSS/u'&g', Pan-STARRS (PS1), 2MASS, WISE/W1&W2, WISE/W3, GALEX, and APASS in order. In addition, the saturation magnitude is set to be 14 for the PS1 and SDSS photometric results. The quality flag in PS1 is required to be 16, representative of good quality in the stack; the quality flags "Q" and "q_mode" in SDSS are required to be 3 and "+", respectively, for selecting the most reliable data.

For spectroscopic data from LAMOST, quality control is put on $T_{\rm eff}$ and $\log g$. For the A-type star catalog, the relative error of temperature $\sigma_{T_{\rm eff}}/T_{\rm eff}$ is required to be less than 10%. While for OB stars, no further quality control on effective temperature is adopted because the error of $T_{\rm eff}$ is unavailable. Meanwhile, $\log g$ is constrained to >3.5 to pick up the dwarf stars for both the catalogs by taking account of the Kiel Diagram (Figure 1), following the suggestion by Worley et al. (2016). The giant stars are not studied because their sample is too small to suit the blue-edge method. On the metallicity, it has little effect on the intrinsic colors in infrared (Bessell & Brett 1988). In the optical, the metallicity effect starts to appear, while it becomes large for the UV bands (Sun et al. 2018). Unfortunately, the catalog for OB stars ($T_{\rm eff} > 10{,}000$ K) provides no measurement of stellar metallicity. Nevertheless, OB stars are generally young in the Galactic thin disk and thus metal-rich like the Sun. It would be reasonable to assume that the OB stars share the same metallicity with the Sun, i.e., [Fe/H] = 0. Accordingly, a criteria of $-1 <$ [Fe/H] < 1 is set for A-type stars (Figure 2) and not further divided.

The final number of stars in each sample to determine the color indexes are listed in Table 1, and they are decoded by the black dots in Figure 1 where the gray dots decode the stars dropped in further analysis.

3. The Blue-edge Method

Following the method of Wang & Jiang (2014), Xue et al. (2016), Jian et al. (2017), and Sun et al. (2018), we make use of the blue-edge method to determine intrinsic colors of early-type stars from the selected sample above. The key step is to find the blue edge in the $T_{\rm eff}$–color diagrams for the intrinsic color index. Although this method seems to be mature after a series of applications, the application on early-type stars presents some new problems. The details of our procedure are as follows.

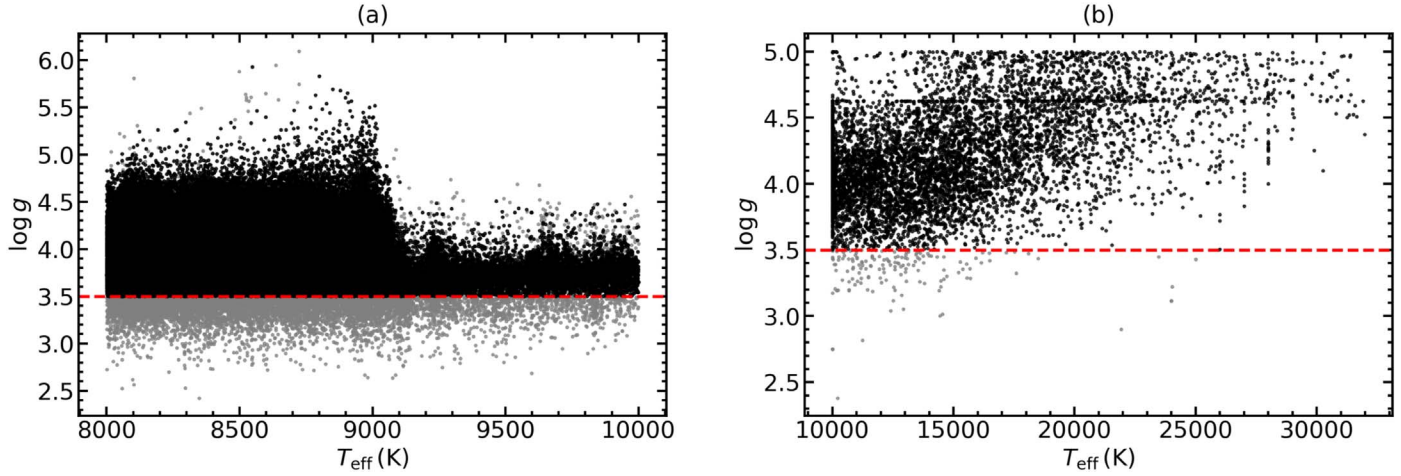

Figure 1. Kiel Diagrams for (a) the A-type star and (b) the OB star catalogs. The red line refers to the limit for log g. The gray points denote the original sample and the black points the selected sample according to the criteria of log g and [Fe/H].

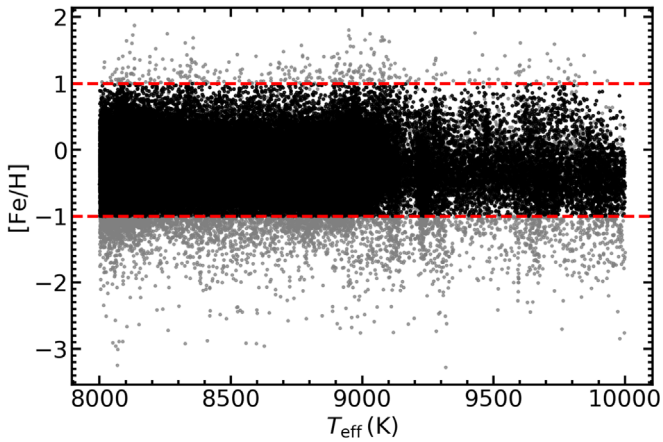

Figure 2. [Fe/H] distribution of the stars from the A-type star catalog. The red dashed lines mark our criteria of $-1 <$ [Fe/H] < 1. The gray points denote the original sample and the black points the selected sample according to the criteria of log g and [Fe/H].

1. Divide the sample into some bins according to $T_{\rm eff}$ in the $T_{\rm eff}$–color diagram. The number of sources are very different at different temperatures due to both observational bias and intrinsic non-homogenous distribution (the number of early-type stars is less than that of late-type stars), thus we take a variable bin size. For $T_{\rm eff}$ from 8000 to 10,000 K (i.e., A-type stars) where a great number of stars (about 10^5 sources for each color index) are observed, a size of 50 K is adopted. While for the hotter (i.e., O- and B-type) stars, the sample is significantly smaller. A bin size of 500 K and 5000 K is adopted for $T_{\rm eff} \in$ (10,000, 16,000 K) and $T_{\rm eff} >$ 16,000 K, respectively. In addition, a sliding window with a step of 1000 K is used to compensate for the scarcity of bin numbers after 16,000 K. Although we are compelled to adopt such a big bin size, there should be little effect because intrinsic color indices change slowly with $T_{\rm eff}$ at the high $T_{\rm eff}$ end. As Table 1 shows, the cross-identified sample between GALEX/NUV and APASS/B has only 2669 sources, for which a special bin size of 2000 K from 10,000 to 16,000 K is used to include more stars in an individual bin.
2. Discard the bins with <10 stars because the small number would lead to very uncertain definition of the blue edge. For $u' - g'$, those bins at $T_{\rm eff} \in$ [8000, 10,000] K with <50 stars are discarded to match the photometric quality of SDSS/u'&g'.
3. Practically, the bluest bottom in the $T_{\rm eff}$–color diagram is not the real intrinsic color. Due to the photometric uncertainty, the observed color will be either bluer or redder than its true color by the amount of photometric error, which leads to a distribution of the color index on the bluer side of intrinsic color. Therefore, we take some percentage (X%) of the bluest colors as the non-reddening region of each bin. Jian et al. (2017) discussed the difference among choosing 3%, 5%, and 10% bluest stars, and concluded that the differences of color indexes are within 0.02 mag for A- to M-type stars in 2MASS/J − 2MASS/H, which is smaller than the photometric error. Meanwhile, Wang & Jiang (2014), Xue et al. (2016), and Jian et al. (2017) all chose 5%. We take a slightly different strategy. For $T_{\rm eff}$ between 8000 and 10,000 K, we follow the convention, i.e., choosing the 5% bluest. While for $T_{\rm eff} >$ 10,000 K, 1% is chosen. This change is made to coincide with the selection effect. The OB stars become intrinsically bright with high $T_{\rm eff}$ (here >10,000 K). If they experience no interstellar extinction, which means they are nearby, they are apparently very bright and easily become saturated in photometry, in particular in the optical bands. In such case, they are removed by our quality control processing. Consequently, the remained sample would contain a smaller portion of stars with zero-reddening. The choice of the boundary temperature is somehow arbitrary, but 10,000 K marks the borderline between A-type and OB-type stars and also between the two catalogs. It can be anticipated that this change would bring about some discontinuity of the median values of the colors around 10,000 K, but it is small and being smoothed very well by the analytic fitting (see the next section and Figure 4).
4. Clip the points with a 3σ rule after a Gaussian fitting is performed to each bin sample of stars, afterwards the median of the remaining points is taken as the intrinsic color of the corresponding bin.
5. Fit the blue-edge points by the function

$$C^0_{\lambda_1,\lambda_2} = A \cdot \exp\left(-B \cdot \frac{T_{\rm eff}}{10{,}000\ {\rm K}}\right) + C.$$

Table 1
Number of Stars in the Final Sample for Various Color Indexes

Color Index	$C_{G_{BP},G_{RP}}$	$C_{u',g'}$	$C_{g,r}$	$C_{r,i}$	$C_{i,z}$	$C_{z,y}$	$C_{J,H}$	$C_{H,Ks}$	$C_{J,W1}$	$C_{J,W2}$	$C_{J,W3}$	$C_{B,V}$	$C_{NUV,B}$
Total numbers	140418	9391	55169	52071	50774	48682	67245	80158	99287	73655	7339	38760	2668

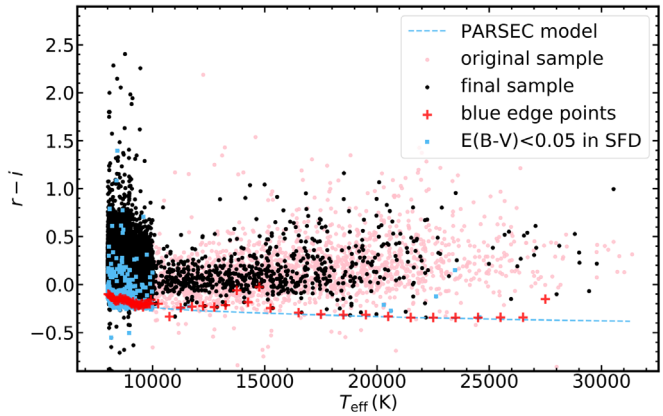

Figure 3. Color–$T_{\rm eff}$ diagram for PS1$/r$ − PS1$/i$. The original sample is decoded by pink dots and the final sample by black dots. The median value of the bluest 5% for $T_{\rm eff} < 10{,}000$ K and 1% for $T_{\rm eff} > 10{,}000$ K are denoted by red crosses. In comparison, the intrinsic colors calculated by the PARSEC model are displayed by a blue dashed line and the stars with $E(B-V) < 0.05$ in the SFD dust map are displayed by blue squares.

Although the form of the fitting function is not important, the exponential form is chosen since a monotonously decreasing relation of the color index with $T_{\rm eff}$ is expected for a blackbody radiation that is a very good approximation for early-type stars.

Figure 3 takes the color index PS1$/r$ − PS1$/i$ as an example to illustrate the method, where the black dots are the sample stars after quality control and the pink dots are from the original sample. It can be seen that many of bluest stars with $T_{\rm eff} > 10{,}000$ K are removed after quality control mostly due to a saturation problem, which made us shift the percentage to 1% when choosing the zero-reddening stars. The median value of $r-i$ of the bluest 5% (for $T_{\rm eff} < 10{,}000$ K) or 1% (for $T_{\rm eff} > 10{,}000$ K) displays some deviations from the general tendency around 10,000 and 16,000 K. The deviation around 10,000 K is caused by the change of the percentage, and that around 16,000 K is caused by the change of the bin width for which a large bin width and a sliding window is taken for $T_{\rm eff} > 16{,}000$ K to compensate for the reduction of the number of stars. But these deviations have little effect on the final fitting curve, which can be seen from Figure 4. The relation of the intrinsic color index with $T_{\rm eff}$ is compared with the PARSEC model, and a very good agreement is found both in Figures 3 and 4. As Sun et al. (2018) obtained the results by taking the very low-extinction stars from the SFD (taken from the initial characters of the authors' names of the paper Schlegel et al. 1998b) dust map (Schlegel et al. 1998a, 1998b; Schlafly & Finkbeiner 2011), which is very consistent with the blue-edge method, we checked the stars with $E(B-V) < 0.05$ mag in the SFD map. It can be seen from Figure 3 that many of these stars suffer some amount of extinction and few OB stars are of low extinction, which can be understood that these early-type stars are located in a place further than the dust cloud traced by the SFD map, proving that they are distant. The method of taking the low-extinction stars from the SFD map works no more for the OB-type stars.

Figure 4 displays the color–$T_{\rm eff}$ diagrams for all the studied color indexes, where the symbols follow the convention of Figure 3. In addition, the fitting curves from the blue-edge method are present as well as the result from the PARSEC model calculation.

The color index $B-V$ is dealt with in a way slightly different from the other color indexes. The blue-edge points selected by the above criteria are apparently redder than the expectation from the PARSEC model, which is remarkable. After all, the color index $u'-g'$ should be more susceptible to extinction than $B-V$, but it shows high consistency with the PARSEC model. The color index $g-r$ is very similar to $B-V$ as neither deviate from the PARSEC model. As discussed above, it may be caused by the exclusion of high-temperature, zero-reddening stars due to the saturation problem. To testify this possibility, all the APASS stars with $T_{\rm eff} > 10{,}000$ K are included, i.e., no quality control is applied except to those without error assignment. The newly determined curve (red solid line in Figure 5) is consistent with the PARSEC model, with a goodness comparable to other visual color indexes. This result may imply that the photometry quality control was too severe for the APASS catalog. Another problem with $B-V$ is that a single exponential function cannot match the selected blue-edge points well. In order to reflect the true trend, a linear function ($C^0_{B,V} = A \cdot \frac{T_{\rm eff}}{10{,}000\ {\rm K}} + B$) is introduced. Specifically, an exponential function is fitted for the points with $T_{\rm eff} < 16{,}000$ K, and a linear function is fitted for the points with $T_{\rm eff} > 10{,}000$ K. The points with $T_{\rm eff} \in [10{,}000,\ 16{,}000]$ are adopted to fit both the exponential and linear functions, which approximate each other closest at about 13,000 K, with a difference of $\simeq$0.02 mag. So the final result takes the exponential curve at $T_{\rm eff} < 13{,}000$ K and the linear curve at $T_{\rm eff} > 13{,}000$ K, and the average color of them at $T_{\rm eff} = 13{,}000$ K is adopted. The comparison with $u'-g'$ and $g-r$ in Figure 5 shows a reasonable consistency.

The color index NUV − B is treated specially and shown in Figure 6. As we mentioned above, a bin size of 2000 K instead of 500 K is adopted for NUV − B in the range of 10,000–16,000 K. Moreover, the number of stars with $T_{\rm eff} > 16{,}000$ K decreases sharply and there is no possibility to define some blue-edge points there. For a complete coverage of the temperature, we pick up the three bluest stars (denoted by crosses in Figure 6) and correct the interstellar extinction to obtain their intrinsic color indexes. According to the SFD dust map, the $E(B-V)$ toward their sightlines is $\sim$0.05 ($E(B-V) \approx 0.05$). In addition, these three stars have high Galactic latitude that supports the correctness of the low extinctions. From the average relation $E({\rm NUV}-B)/E(B-V) = 3.77$ by Sun et al. (2018), their intrinsic NUV − B is calculated. Certainly the result depends on the accuracy of the photometry and spectroscopy of the three stars and may suffer bigger uncertainty in comparison with other color indexes. But the data is limited by the observation, and this is the reliable result achievable up to date.

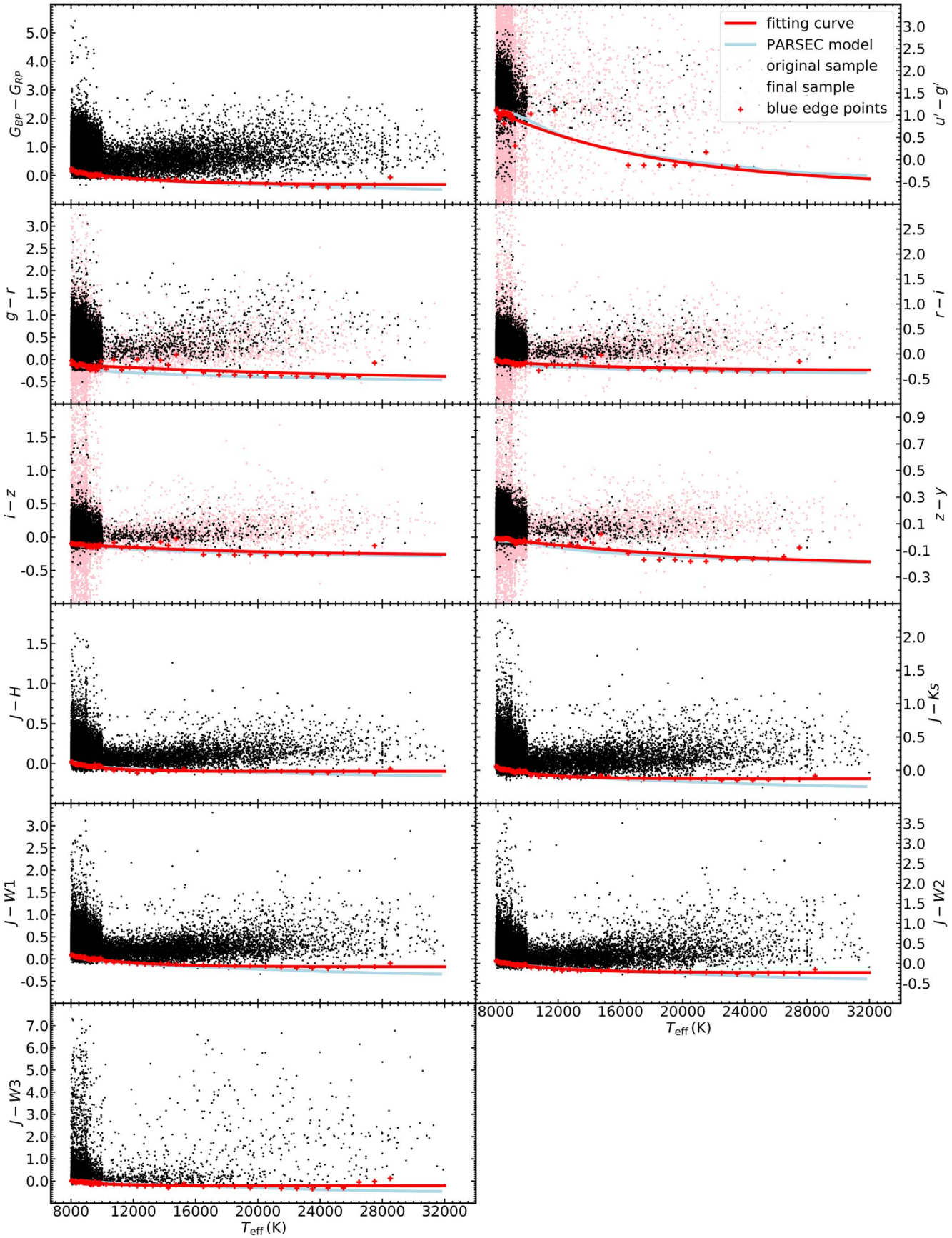

Figure 4. Color–$T_{\rm eff}$ diagram for the studied color indexes. The original sample is decoded by pink dots and the final sample by black dots. The median value of the bluest 5% for $T_{\rm eff} < 10{,}000$ K and 1% for $T_{\rm eff} > 10{,}000$ K are denoted by red crosses. In comparison, the intrinsic colors calculated by the PARSEC model are displayed by a light blue line.

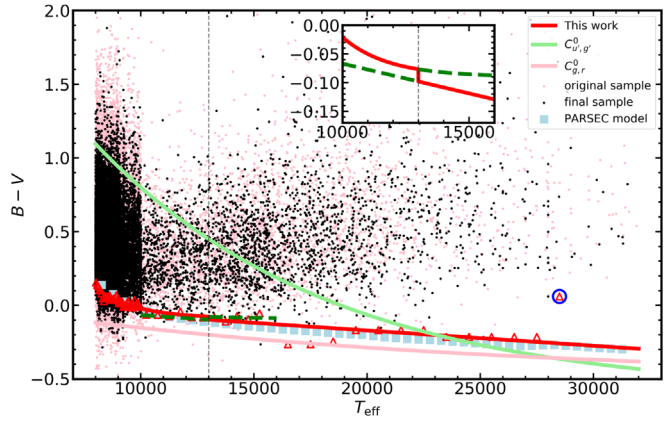

Figure 5. $B-V$ vs. $T_{\rm eff}$ diagram. For $T_{\rm eff} > 16{,}000$ K, the median value of the bluest 0.1% is chosen to be the blue-edge points, which also represent the bluest points in each bin. The exponential fit curve and linear fit line are adopted before and after 13,000 K, respectively. For the intrinsic color at $T_{\rm eff} = 13{,}000$ K, the average of these two fitting curves is adopted. The intrinsic colors of $u'-g'$ and $g-r$ of this work are also present. The red point at the highest temperature with a blue circle is not included in the fitting. The inset displays the common part used in the two functions where the green dashed line denotes the part of each line that is rejected. The other symbols follow the convention of Figure 4.

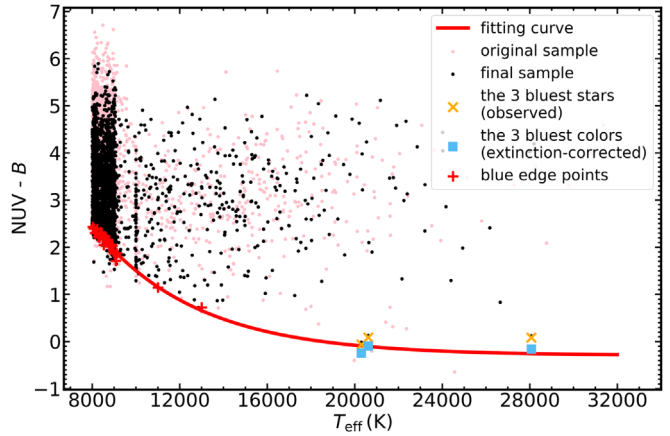

Figure 6. NUV $-$ B vs. $T_{\rm eff}$ diagram. The three bluest stars with $T_{\rm eff} > 16{,}000$ K are chosen and corrected for interstellar extinction according to the $E(B-V)$ from the SFD dust map and the extinction law of Sun et al. (2018). The other symbols follow the convention of Figure 4.

4. Results and Discussions

The results are presented in Figures 4–6 to show the selection and fitting of the blue edge, and Table 2 for the fitting coefficients to the exponential function and the linear function for $C^0_{B,V}$ at $T_{\rm eff} > 13{,}000$ K. The intrinsic color indexes of spectral type O9-A5 are listed in Table 3.

For the color indexes in the SDSS and Pan-STARRS1 bands, i.e., $u'-g'$, $g-r$, $r-i$, $i-z$, and $z-y$, the number of stars decreases apparently after quality control as shown in Figure 4. Like the case we have explained for $r-i$ in Figure 3, the decreasing is caused by discarding the saturated stars that are nearby and bright thus a little reddened. Nevertheless, the blue edge is very consistent with the PARSEC model and the result should be reliable. It deserves mentioning that the coincidence of $u'-g'$ with the PARSEC model is somehow accidental. Due to the small number of stars at high temperature and possibly the decreasing accuracy of photometry for bright stars, it can be seen from Figure 4 that the selected blue-edge points

Table 2
Coefficients of the Function for Fitting the Relation of the Intrinsic Color with $T_{\rm eff}$

Colors	A	B	C
$C^0_{G_{\rm BP},G_{\rm RP}}$	2.442	2.048	−0.318
$C^0_{u',g'}$	3.648	0.955	−0.604
$C^0_{g,r}$	0.566	0.486	−0.501
$C^0_{r,i}$	0.439	1.105	−0.335
$C^0_{i,z}$	0.362	0.906	−0.278
$C^0_{z,y}$	0.387	0.732	−0.222
$C^0_{J,H}$	3.662	4.392	−0.095
$C^0_{J,Ks}$	2.555	3.366	−0.128
$C^0_{J,\rm W1}$	2.023	2.581	−0.175
$C^0_{J,\rm W2}$	2.298	2.623	−0.229
$C^0_{J,\rm W3}$	6.397	4.211	−0.216
$C^0_{B,V}$ (exponential)	17.546	5.539	−0.090
$C^0_{B,V}$ (linear)	−0.116	0.051	
$C^0_{\rm NUV,B}$	14.962	2.118	−0.295

Note. The first row for $C^0_{B,V}$ is the coefficients for the exponential function ($C^0_{\lambda_1,\lambda_2} = A \cdot \exp\left(-B \cdot \frac{T_{\rm eff}}{10{,}000\ {\rm K}}\right) + C$) at $T_{\rm eff} < 13{,}000$ K, while the second row is for the linear function ($C^0_{B,V} = A \cdot \frac{T_{\rm eff}}{10{,}000\ {\rm K}} + B$) adopted at $T_{\rm eff} > 13{,}000$ K. Other coefficients are all for the exponential function.

are not numerous enough to trace the trend completely of the color change with $T_{\rm eff}$ even with some relaxed constraint to the data. We would rather conclude that the result of $u'-g'$ is not in conflict with the PARSEC model. On the other hand, the $G_{\rm BP}-G_{\rm RP}$ is much less affected by the saturation problem. The infrared bands have no problem of saturation either.

4.1. Comparison with Other Results

The result on $J-H$ is compared with previous works in Figure 7. Since this is an extension to the high temperature of the work by Jian et al. (2017), a smooth connection is expected. It can be seen that the connection with Jian et al. (2017) is pretty good, with a difference of about 0.02 mag at the joining point. It should be noted that Jian et al. (2017) used a third-order polynomial function to express the change of the color index with $T_{\rm eff}$ while this work uses an exponential function, so that the two curves have different slopes and no extrapolation should be made to either side. However, it is clear that our results show larger uncertainties at this joining point. Therefore, for those stars with $T_{\rm eff} \approx 8000$ K, such as A5-type stars (8160 K according to Tokunaga 2002), we suggest the use of the blue-edge points (decoded as red triangles in Figure 7) as the intrinsic colors. That is to say, the average colors of three blue-edge points (at 8125, 8175, and 8225 K) are adopted to represent the intrinsic colors of A5-type stars (see Table 3). On the other hand, the derived color index is slightly redder than that calculated from the PARSEC model. But Koornneef (1983), Bessell et al. (1998), and Wegner (2014) also obtained a redder $J-H$ than the PARSEC model, which brought about their agreement with our result, in particular at the high-temperature end. The other infrared color indexes, $J-Ks$, $J-$W1, and $J-$W2 are all slightly redder at the high-temperature end than the PARSEC model. It should be noted that Bessell et al. (1998) determined intrinsic colors for OB dwarfs using the model atmosphere ATLAS9 convolved with

Table 3
Intrinsic Color Indices According to Spectral Types[a]

Spectral Type	$C^0_{G_{BP},G_{RP}}$	$C_{u',g'}$	$C^0_{g,r}$	$C^0_{r,i}$	$C^0_{i,z}$	$C^0_{z,y}$	$C^0_{J,H}$	$C^0_{J,Ks}$	$C^0_{J,W1}$	$C^0_{J,W2}$	$C^0_{J,W3}$	$C_{B,V}$	$C^0_{NUV,B}$	T_{eff}
O9	−0.32	−0.44	−0.38	−0.32	−0.26	−0.19	−0.09	−0.13	−0.17	−0.23	−0.22	−0.33	−0.28	32500
B0	−0.31	−0.42	−0.38	−0.32	−0.26	−0.18	−0.09	−0.13	−0.17	−0.23	−0.22	−0.31	−0.28	31500
B1	−0.31	−0.29	−0.34	−0.31	−0.24	−0.16	−0.09	−0.13	−0.17	−0.23	−0.22	−0.25	−0.23	25600
B2	−0.29	−0.17	−0.31	−0.30	−0.23	−0.15	−0.09	−0.13	−0.17	−0.22	−0.22	−0.21	−0.16	22300
B3	−0.27	−0.01	−0.28	−0.28	−0.21	−0.13	−0.09	−0.12	−0.16	−0.21	−0.21	−0.17	−0.03	19000
B4	−0.25	0.10	−0.26	−0.27	−0.20	−0.11	−0.09	−0.12	−0.15	−0.20	−0.21	−0.15	0.10	17200
B5	−0.21	0.23	−0.23	−0.25	−0.19	−0.10	−0.09	−0.11	−0.14	−0.19	−0.21	−0.13	0.28	15400
B6	−0.18	0.34	−0.22	−0.24	−0.18	−0.08	−0.09	−0.11	−0.12	−0.17	−0.20	−0.11	0.46	14100
B7	−0.15	0.45	−0.20	−0.23	−0.17	−0.07	−0.08	−0.10	−0.10	−0.15	−0.19	−0.08	0.66	13000
B8	−0.10	0.58	−0.18	−0.22	−0.15	−0.06	−0.07	−0.08	−0.08	−0.12	−0.17	−0.06	0.93	11800
B9	−0.05	0.71	−0.16	−0.20	−0.14	−0.05	−0.06	−0.06	−0.05	−0.09	−0.15	−0.04	1.26	10700
A0	0.03	0.87	−0.14	−0.18	−0.12	−0.03	−0.04	−0.02	0.00	−0.04	−0.10	0.00	1.71	9480
A2	0.08	0.97	−0.13	−0.17	−0.12	−0.02	−0.02	0.00	0.03	0.00	−0.06	0.04	2.02	8810
A5	0.17	1.08	−0.08	−0.13	−0.10	−0.01	0.01	0.04	0.07	0.04	−0.01	0.12	2.36	8160

Note. As suggested in Section 4.1, the intrinsic colors for A5-type stars are from the blue-edge points instead of the fitting curve.
[a] The relation between spectral type and T_{eff} follows the Allen's definition (Tokunaga 2002).

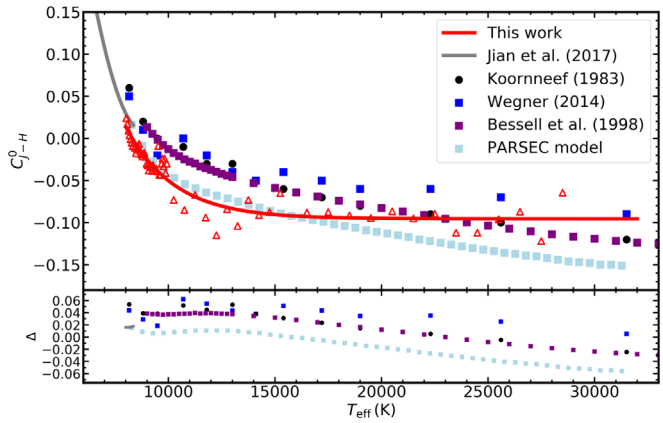

Figure 7. Comparison of the derived intrinsic color index C^0_{J-H} with previous works. The lower panel shows the difference $\Delta = C^0_{\rm PreviousWork} - C^0_{\rm ThisWork}$.

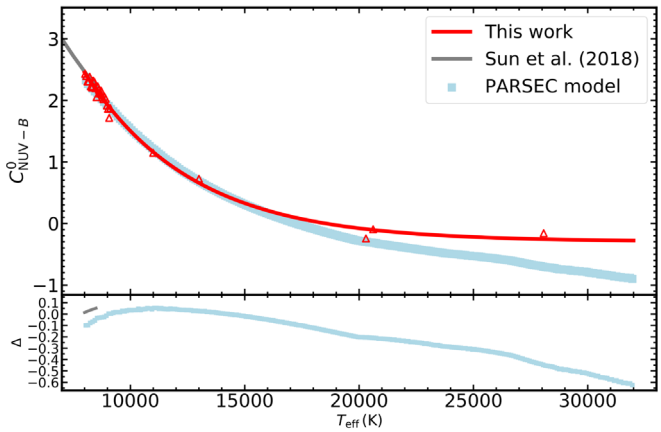

Figure 8. Comparison of the derived intrinsic color index C^0_{NUV-B} with Sun et al. (2018) and the PARSEC model with [Fe/H] = 0. The lower panel shows the difference $\Delta = C^0_{\rm PreviousWork} - C^0_{\rm ThisWork}$.

the filter response functions with $\log g$ of 4, 4.5, and 5, respectively. Since we selected dwarfs by $\log g > 3.5$, the average color from the three surface gravities are compared in Figure 7, which is also based on the fact that the intrinsic colors with $\log g \in [4, 5]$ are more or less the same. Apparently $J - H$ from Bessell et al. (1998) is redder than the PARSEC model by about 0.03 mag despite the fact that they used the same method.

Similar to the case of $J - H$, the color index, NUV $- B$, is an extension to the high temperature of Sun et al. (2018) that is compared in Figure 8. Although NUV $- B$ is sensitive to metallicity (Sun et al. 2018), we make no division of metallicity because it is not measured for the LAMOST OB stars. Fortunately OB stars are young massive stars and should be solar-like and metal-rich. So if the case of $-0.125 <$ [Fe/H] < 0.125 from Sun et al. (2018) is taken for comparison, the result is in good agreement. Again, the color is redder than the PARSEC model at the high-temperature end, like the case of $J - H$. Unfortunately, no other work on NUV $- B$ is available at this temperature range. Since the blue edge is very difficult to define here, this discrepancy may be caused our overestimation of the color index. Meanwhile, the stellar model in the ultraviolet may suffer some uncertainty as well.

The color index $B - V$ agrees with previous work in general as shown in Figure 9 in that the difference is mostly smaller than 0.05 mag. The coincidence is high with Fitzgerald (1970), Flower (1977), Bessell et al. (1998), and the PARSEC model. Meanwhile, the result of Wegner (1994) seems to be redder than ours in particular at the high-temperature end, which approaches our line of $u' - g'$; nevertheless this difference is small and acceptable.

It should be mentioned that the optical color indexes are in very good agreement with the PARSEC model with no systematic deviations.

4.2. The O-type Stars

It can be seen from Table 3 that the LAMOST catalogs contain mostly A- and B-type stars. Concerning O-type stars, only the very late-O type (O9) is included, and thus the majority of the O-type is missed. For the completeness of this work, a sample of O-type stars is needed. As mentioned in Section 1, GOSSS is the largest catalog of pure O-type stars to date that provides the spectral class but no T_{eff} of the stars. In order to use the GOSSS sample by the blue-edge method, the spectral type should be converted to the T_{eff}. This is done by

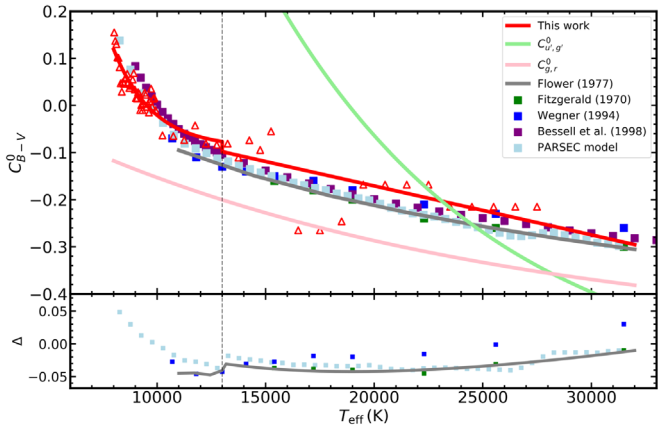

Figure 9. Comparison of the derived intrinsic color index C^0_{B-V} with previous works. The lower panel shows the difference $\Delta = C^0_{\rm PreviousWork} - C^0_{\rm ThisWork}$.

calculating the average $T_{\rm eff}$ for each sub-type in Massey et al. (2009). It should be mentioned that GOSSS determined the spectral types of some stars as O9.2 or O9.7 but the $T_{\rm eff}$ for these two types are not available in Massey et al. (2009), so we adopted the rounding principle to approximate O9.2, O9.7 as O9, O9.5, respectively. Furthermore, a few stars do not have an accurate spectral type (marked as O4-5, etc.). In this case, the former type (with higher $T_{\rm eff}$) is chosen to be its final type. Figure 10 shows the results in four colors ($G_{\rm BP} - G_{\rm RP}$, $g - r$, $J - H$, and $J -$ W1). Since O-type stars are even more luminous than A- and B-type stars, they are mostly distant and suffer some interstellar extinction, thus there is little possibility to find zero-reddening stars in the sample. Similar to what we have done for the NUV $- B$ color, we checked the bluest colors and the colors after correcting for the extinction of the stars with $E(B-V) < 0.05$ mag from the SFD dust map. The conversion factors from $E(B-V)$ are $E(G_{\rm BP}-G_{\rm RP})/E(B-V) = 1.321$ and $E(J-{\rm W1})/E(B-V) = 0.686$ from Wang & Chen (2019), and $E(g-r)/E(B-V) = 1.018$ and $E(J-H)/E(B-V) = 0.260$ from Schlafly & Finkbeiner (2011). The locations of so-derived "intrinsic colors" in Figure 10 obey no clear law, and the lack of such stars is evident at high temperatures as expected. Instead, the extrapolation of our analytic function of the relation between intrinsic color and $T_{\rm eff}$ (red line in Figure 10) seems to be able to delineate the tendency of the blue edge until the high edge of $T_{\rm eff}$. Therefore, we recommend the use of our analytic relations to the O-type stars even though the uncertainty should be borne in mind.

4.3. The Supergiants

It has been well known in previous works that the intrinsic colors of supergiants and dwarfs differ significantly. This work focuses on the OB dwarfs. Since giants or supergiants are redder than dwarfs, the small amount of giants or supergiants that may be presented in the final sample after the data quality control would not change the intrinsic color indexes derived by the blue-edge method in this work.

The LAMOST sample includes supergiant stars in addition to dwarfs from which Liu et al. (2019) determined the luminosity class and spectral type for more than 8000 OB stars. The Liu et al. (2019) catalog contains no stars in class I or I–II, 208 stars in class II, and 498 stars in class II–III. We only take the 208 class II stars as supergiants since class III may be dwarf stars or misclassified. The sample is enlarged by incorporating the supergiant stars from the GOSSS catalog and Hohle et al. (2010) with class I, I–II, and II. After cross-matching with 2MASS, there are 646 supergiants with observed $J - H$, specifically 89, 162, and 395 stars from LAMOST, GOSSS, and Hohle et al. (2010), respectively. For $B - V$, there are 450 supergiants, specifically 81, 112, and 257 stars from LAMOST, GOSSS, and Hohle et al. (2010), respectively. To include more supergiants in the final sample, the errors of B and V are required to be smaller than 0.1 mag instead of 0.05 mag for dwarfs, while the errors of J and H are still required to be less than 0.03 mag. Although the sample is insufficient to determine the intrinsic colors of supergiants by the blue-edge method, the previous results are testified with this new dataset.

The distribution of the OB supergiants sample in the $T_{\rm eff}$ versus color index diagram is displayed in Figure 11 for $J - H$ and $B - V$, where the bluest color in each sub-class is indicated by a red cross. Two obstacles prevent us from determining the intrinsic color by the blue-edge method. One is the very small sample which makes the statistical method invalid. The other is the lack of zero-reddening stars at high-temperature, the O-type stars. This can be understood because the OB supergiants are extremely luminous and mostly locate far in the Galactic plane with unavoidable significant interstellar extinction. Thus the colors are only compared with that of the dwarfs in this work and the supergiants by other works. The data of Bessell et al. (1998) are from the stars with $\log g = 2.5$ and $=3$ at $T_{\rm eff} < 20{,}000$ K and $>20{,}000$ K until 26,000 K respectively. In comparison with the dwarf stars (red curve in Figure 11), it is difficult to draw any very certain conclusion from the data. However, the $(J-H)_0$ of supergiants derived from other works is apparently redder than that of B-type dwarfs. As for O-type stars, the color index $J - H$ of supergiants determined by Wegner (1994) and Martins & Plez (2006) appear to be bluer than dwarfs. For $B - V$, the conclusion is different. While supergiants from other works appear very similar to dwarfs in this work for B-type stars, the results from Wegner (1994) and Martins & Plez (2006) do appear redder than dwarfs for O-type stars, which agree with previous conclusions.

4.4. Uncertainty

Generally the uncertainty of the intrinsic color indexes derived by the blue-edge method comes from three sources: (1) photometric uncertainty, (2) spectroscopic uncertainty, and (3) the uncertainty of fitting the relation of the color index with $T_{\rm eff}$. As analyzed in Jian et al. (2017), source (3) mainly comes from how much percent of the bluest stars should be selected to represent the blue edge, which is usually less than the photometric error and negligible. Then the uncertainty of the intrinsic color index $\varepsilon^0_{C_{\lambda_1,\lambda_2}}$ between band λ_1 and λ_2 can be written as

$$\varepsilon^0_{C_{\lambda_1,\lambda_2}} = \sqrt{\varepsilon^2_{\lambda_1} + \varepsilon^2_{\lambda_2} + \varepsilon^2_{T_{\rm eff}}},$$

where ε_{λ_1} and ε_{λ_2} refer to the uncertainties from photometry in band λ_1 and λ_2, respectively, and $\varepsilon_{T_{\rm eff}}$ refers to the uncertainty brought by the error of $T_{\rm eff}$. ε_{λ_1} and ε_{λ_2} are chosen to be the upper limits of the photometric errors (σ_{λ_1} and σ_{λ_2} described in Section 2). As we choose 10% as the constraint of the relative error of temperature, the upper limit of $T_{\rm eff}$ is about 1000 K in the early-A type stars catalog. Unfortunately, the OB stars

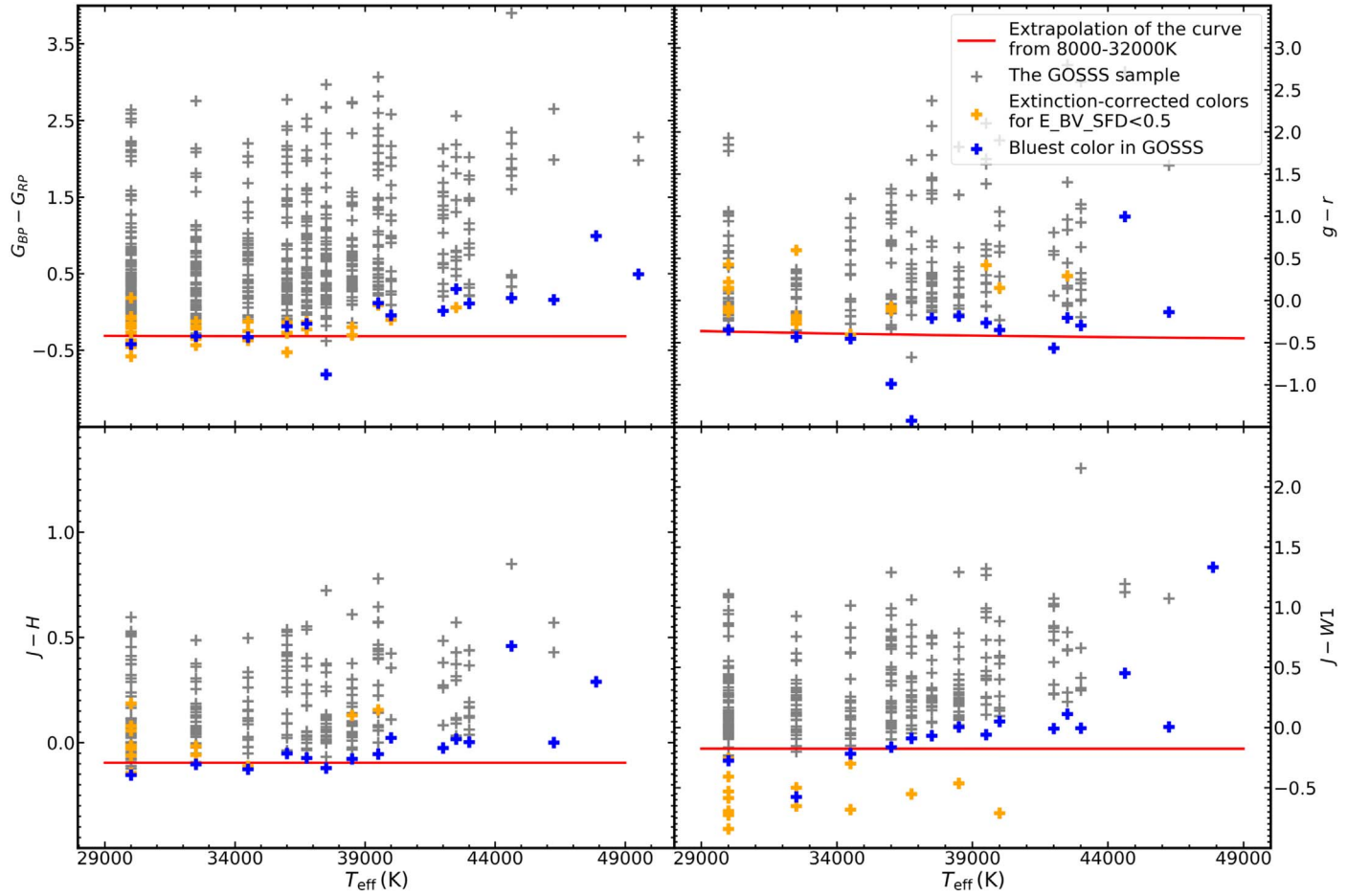

Figure 10. Color–$T_{\rm eff}$ diagram for the O-type stars in the GOSSS catalog. The gray, blue, and orange cross denote the GOSSS sample stars, the bluest star in each subtype and the color index for stars with $E(B-V)<0.5$ after correcting for the interstellar extinction according to the $E(B-V)$ from the SFD dust map. The red line is the extrapolation from the fitting curves based on the sample of A- and B-type stars.

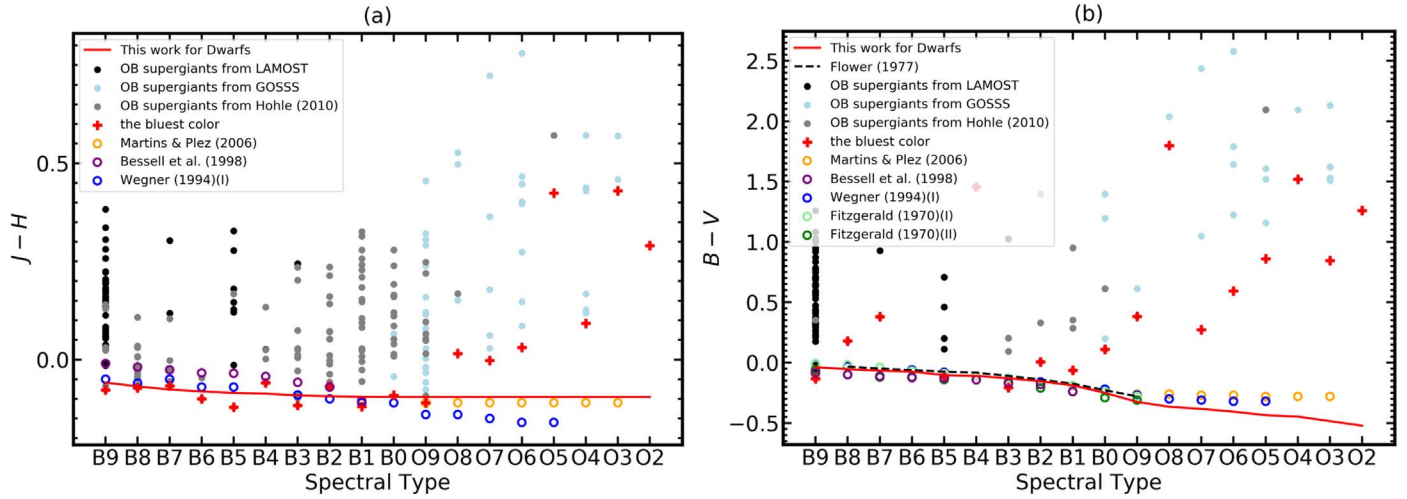

Figure 11. Color–spectral type diagram for the supergiants (with luminosity class I, I–II, and II). The black, light blue, and gray dots are the OB supergiants from LAMOST, GOSSS, and Hohle et al. (2010), respectively. The red crosses denote the bluest color for each sub-type. Previous works are presented as circles. The red lines indicate intrinsic colors of dwarfs by this work.

catalog has no information on the error of $T_{\rm eff}$. According to the results of the intrinsic colors (Figure 4), the difference of 1000 K in $T_{\rm eff}$ leads to a difference of about 0.02 mag in all the color indexes except NUV $-$ B. For NUV $-$ B, this difference rises to about 0.2 mag, which is taken to be the value of $\varepsilon_{T_{\rm eff}}$ for NUV $-$ B. For other color indexes, 0.02 is used for $\varepsilon_{T_{\rm eff}}$. The

Table 4
Uncertainties of Intrinsic Color Indices

Uncertainties	$C_{G_{BP},G_{RP}}$	$C_{u',g'}$	$C_{g,r}$	$C_{r,i}$	$C_{i,z}$	$C_{z,y}$	$C_{J,H}$	$C_{H,Ks}$	$C_{J,W1}$	$C_{J,W2}$	$C_{J,W3}$	$C_{B,V}$	$C_{NUV,B}$
ε_{λ_1}	0.01	0.05	0.02	0.02	0.02	0.02	0.03	0.03	0.03	0.03	0.03	0.05	0.10
ε_{λ_2}	0.01	0.05	0.02	0.02	0.02	0.02	0.03	0.03	0.03	0.03	0.05	0.05	0.05
$\varepsilon_{T_{\rm eff}}$	0.02	0.02	0.02	0.02	0.02	0.02	0.02	0.02	0.02	0.02	0.02	0.02	0.20
$\varepsilon^0_{C_{\lambda_1,\lambda_2}}$	0.024	0.073	0.035	0.035	0.035	0.035	0.047	0.047	0.047	0.047	0.062	0.073	0.229

calculated uncertainty are presented in Table 4. The error is ∼0.03 mag in the optical, ∼0.05 mag in the near-infrared, and ∼0.2 mag in NUV − B.

5. Summary

By using the newly released largest photometric and spectroscopic catalogs for early-type stars, we determined their intrinsic color indices from the near-ultraviolet to infrared bands, namely Gaia/G_{BP}, G_{RP}, SDSS/u', g', PS1/g, r, i, z, y, 2MASS/J, H, K_S, WISE/W1, W2, W3, GALEX/NUV, and APASS/B, V. The blue-edge method used results in an analytic relation of the intrinsic color index with the effective temperature $T_{\rm eff}$ for B- and A-type stars. Our results agree well with the PARSEC model in the optical. Meanwhile, the derived intrinsic color indexes at the high-temperature end are redder than the PARSEC model in the $B - V$, infrared, and NUV − B. The investigation of the GOSSS O-type stars seems to indicate that the derived relations of intrinsic colors with $T_{\rm eff}$ can be extrapolated to O-type stars. Our new data and results also support the intrinsic colors of B-type supergiants determined by previous work.

Both Dingshan Deng and Yang Sun contributed equally to this paper. We are very grateful to Profs. Wenyuan Cui and Chao Liu for their helpful discussions. We also thank the referee for the suggestions. This work is supported by the National Natural Science Foundation of China through the projects NSFC 11533002, 11603002, and Beijing Normal University grant No. 310232102. This work has made use of data from the surveys by LAMOST, Gaia, SDSS, APASS, Pan-STARRS1, 2MASS, WISE, and GALEX. For the SFD dust map (Schlegel et al. 1998b), we made use of the Python interface by Green (2018).

ORCID iDs

Biwei Jiang https://orcid.org/0000-0003-3168-2617

References

Alam, S., Albareti, F. D., Prieto, C. A., et al. 2015, ApJS, 219, 12
Bessell, M. S. 2005, ARA&A, 43, 293
Bessell, M. S., & Brett, J. M. 1988, PASP, 100, 1134
Bessell, M. S., Castelli, F., & Plez, B. 1998, A&A, 337, 321
Bressan, A., Marigo, P., Girardi, L., et al. 2012, MNRAS, 427, 127
Chambers, K. C., Magnier, E. A., Metcalfe, N., et al. 2016, arXiv:1612.05560
Chen, B.-Q., Liu, X.-W., Yuan, H.-B., et al. 2014, MNRAS, 443, 1192
Code, A. D., Bless, R. C., Davis, J., & Brown, R. H. 1976, ApJ, 203, 417
Cui, X.-Q., Zhao, Y.-H., Chu, Y.-Q., et al. 2012, RAA, 12, 1197
Cutri, R. M., Al, E., et al. 2013, yCat, 2328, 0
Ducati, J. R., Bevilacqua, C. M., Rembold, S. B., & Ribeiro, D. 2001, ApJ, 558, 309
Fitzgerald, M. P. 1970, A&A, 4, 234
Flower, P. J. 1975, A&A, 41, 391
Flower, P. J. 1977, A&A, 54, 31
Gaia Collaboration, Brown, A. G. A., Vallenari, A., et al. 2018, A&A, 616, A1
Gaia Collaboration, Prusti, T., de Bruijne, J. H. J., et al. 2016, A&A, 595, A1
Garcia-Segura, G., Mac Low, M.-M., & Langer, N. 1996, A&A, 305, 229
Gontcharov, G. A. 2008, AstL, 34, 7
Gontcharov, G. A. 2012, AstL, 38, 694
Green, G. 2018, JOSS, 3, 695
Henden, A., & Munari, U. 2014, CoSka, 43, 518
Henden, A. A., Templeton, M., Terrell, D., et al. 2016, yCat, 2336, 0
Hohle, M. M., Neuhaeuser, R., & Schutz, B. F. 2010, AN, 331, 349
Jian, M., Gao, S., Zhao, H., & Jiang, B. 2017, AJ, 153, 5
Johnson, H. L. 1966, ARA&A, 4, 193
Koornneef, J. 1983, A&A, 500, 247
Krelowski, J., & Strobel, A. 1987, A&A, 175, 186
Kuriliene, G., & Straizys, V. 1977, VilOB, 44, 3
Kurucz, R. L. 1979, ApJS, 40, 1
Lee, T. A. 1970, ApJ, 162, 217
Liu, Z., Cui, W., Liu, C., et al. 2019, ApJS, 241, 32
Mainzer, A., Bauer, J., Grav, T., et al. 2011, ApJ, 731, 53
Maíz Apellániz, J., Sota, A., Arias, J. I., et al. 2016, ApJS, 224, 4
Maíz Apellániz, J., Sota, A., Walborn, N. R., et al. 2011, in Highlights of Spanish Astrophysics VI, ed. M. R. Zapatero Osorio et al. (Spain: SEA), 467
Martin, D. C., Fanson, J., Schiminovich, D., et al. 2005, ApJL, 619, L1
Martins, F., & Plez, B. 2006, A&A, 457, 637
Massey, P., Zangari, A. M., Morrell, N. I., et al. 2009, ApJ, 692, 618
Mohr-Smith, M., Drew, J. E., Napiwotzki, R., et al. 2017, MNRAS, 465, 1807
Papaj, J., Krelowski, J., & Wegner, W. 1993, A&A, 273, 575
Papaj, J., Wegner, W., & Krelowski, J. 1990, MNRAS, 246, 408
Reed, B. C. 2003, AJ, 125, 2531
Schlafly, E. F., & Finkbeiner, D. P. 2011, ApJ, 737, 103
Schlegel, D., Finkbeiner, D., & Davis, M. 1998a, in 14th IAP Meeting, Wide Field Surveys in Cosmology, ed. S. Colombi & Y. Mellier (Gif sur Yvette: Editions Frontieres), 297
Schlegel, D. J., Finkbeiner, D. P., & Davis, M. 1998b, ApJ, 500, 525
Skrutskie, M. F., Cutri, R. M., Stiening, R., et al. 2006, AJ, 131, 1163
Sota, A., Maíz Apellániz, J., Morrell, N. I., et al. 2014, ApJS, 211, 10
Straizys, V. 1987, VilOB, 78, 43
Sun, M., Jiang, B. W., Zhao, H., et al. 2018, ApJ, 861, 153
The, P. S., Wesselius, P. R., & Janssen, I. M. H. H. 1986, A&AS, 66, 63
Tokunaga, A. T. 2002, in Allen's Astrophysical Quantities, ed. A. N. Cox (New York: Springer), 143
Turon, C., Creze, M., Egret, D., et al. 1993, BICDS, 43, 5
Wang, S., & Chen, X. 2019, ApJ, 877, 116
Wang, S., & Jiang, B. W. 2014, ApJL, 788, L12
Wegner, W. 1993, AcA, 43, 209
Wegner, W. 1994, MNRAS, 270, 229
Wegner, W. 2014, AcA, 64, 261
Whittet, D. C. B., & van Breda, I. G. 1980, MNRAS, 192, 467
Worley, C. C., de Laverny, P., Recio-Blanco, A., Hill, V., & Bijaoui, A. 2016, A&A, 591, A81
Wright, C. O., Egan, M. P., Kraemer, K. E., & Price, S. D. 2003, AJ, 125, 359
Wright, E. L., Eisenhardt, P. R. M., Mainzer, A. K., et al. 2010, AJ, 140, 1868
Xiang, M.-S., Liu, X.-W., Yuan, H.-B., et al. 2017, MNRAS, 467, 1890
Xue, M., Jiang, B. W., Gao, J., et al. 2016, ApJS, 224, 23
York, D. G., Adelman, J., Anderson, J. E., Jr., et al. 2000, AJ, 120, 1579